Functional Materials 19, No.4 (2012)

Influence of processing conditions on the structure and properties of yttrium oxide ceramics

V.N.Baumer, M.B.Kosmyna[*], B.P.Nazarenko[*], V.M.Puzikov[*], A.N.Shekhovtsov[*], L.S.Gordienko[**], A.S.Yasukevich[***], N.V.Kuleshov[***], A.E.Gulevich[***], M.P.Demesh[***]

STC "Institute for Single Crystals", Division of Functional Material Chemistry, National Academy of Sciences of Ukraine, 60 Lenin Ave., 61001 Kharkiv, Ukraine

[*]Institute for Single Crystals, STC "Institute for Single Crystals", National Academy of Sciences of Ukraine, 60 Lenin Ave., 61001 Kharkiv, Ukraine

[**]Institute for Scintillation Materials, STC "Institute for Single Crystals", National Academy of Sciences of Ukraine, 60 Lenin Ave., 61001 Kharkiv, Ukraine

[***]Center for Optical Materials and Technologies, Belarusian National Technical University, 65 Nezavisimosty Ave., 220013 Minsk, Republic of Belarus

Received June 31, 2012

By means of "wet" chemistry method Y_2O_3 nanopowder was obtained and characterized by X-ray diffraction analysis and differential thermal analysis. Transparent samples of Y_2O_3 and Y_2O_3:Nd ceramics were produced by vacuum sintering. Granulometric and phase compositions, crystal structure, spectral-kinetic and mechanical properties of the ceramics were studied.

Методом мокрой химии получен нанопорошок Y_2O_3, который охарактеризован методами рентгеновской дифракции и дифференциально-термическим анализом. Спеканием в вакууме получена прозрачная керамика Y_2O_3 и Y_2O_3:Nd. Изучены кристаллическая структура, гранулометрический и фазовый составы, спектрально-кинетические и механические свойства полученной керамики.

1. Introduction

Development of the methods for the obtaining of optical ceramics has resulted in a wide use of the ceramics based on cubic rare earth (RE) oxides as a material for bulbs of gaseous-discharge lamps working at high temperatures, optical windows with a wide transparency range, scintillation detectors, magnetooptical elements [1]. However, the main application field for such ceramics is bound up with active elements of lasers meant for different purposes. An advantage of optical ceramics is the fact that it can be obtained in the form of samples with rather large size and high concentration of impurity uniformly distributed in the bulk, that is hardly possible for single crystals of the corresponding composition. The spectroscopic and generation characteristics of optical ceramics are analogous to those of single crystals, whereas the mechanical characteristic of the former are even better [2]. In particular, the optical ceramics Y_2O_3:Nd was used for creation of laser systems working in different modes [3].

Most of the works aimed at the obtaining of optical ceramics consist of the following

stages: preparation of a nanopowder with given characteristics (morphology, structure type, size dispersion, absence or weak agglomeration), hot isostatic pressing (HIP) or cold isostatic pressing (CIP) with subsequent sintering in vacuum or hydrogen atmosphere at temperatures of about 0.7–0.9 T_{melt}, for example [4, 5]. To obtain YAG ceramics, the authors of [6] applied the method of slip casting instead of HIP or CIP. In [7] Y_2O_3:Nd ceramics was produced by means of uniaxial magnetic pulsed pressing (MIP) of the nanopowder obtained by laser synthesis.

The nanopowder for transparent ceramics processing must comply with certain demands, in particular, be a single-phase, maximally homogeneous and highly dispersed. Therefore, high-purity nanocrystalline powders of high-melting RE oxide compounds with given characteristics as stated above are to be obtained by the methods of "wet" chemistry. Thereat, the method of the obtaining of the initial nanopowder based on pyrolysis of yttrium carbonate $Y_2(CO_3)_3nH_2O$ is considered one of most promising [8].

The present work reports the X-ray diffraction and optical investigations of Y_2O_3 ceramic samples produced by uniaxial pressing and followed vacuum sintering.

2. Experimental

Characterization of the obtained precursor and Y_2O_3 nanopowder was carried out using X-ray powder diffractometry and differential thermal analysis (DTA). The nanopowder and ceramics were studied using a Bragg-Brentano powder diffractometer (SIEMENS D-500, $Cu_{K\alpha}$, λ=1.54184 A). The qualitative phase analysis (XPA) was made using the powder data base "PDF-4 Full File" and the system "EVA" included in the software of the used diffractometer. The quantitative was performed by Rietveld using the program "FullProf" [9]. DTA was realized on a "Derivatograph-C" in air atmosphere.

The procedure for the obtaining of Y_2O_3 nanopowder was the following. Extra pure (high purity) nitrate yttrium salt was deposited using NH_4HCO_3 solution. In the latter nitrate yttrium solution was added drop-by-drop during several hours, the solution pH was maintained on the level of 7–7.5, the reaction mixture temperature was 25°C. Intense liberation of carbon dioxide at the hydrolysis of these compounds promoted additional mixing of the reaction mixture and

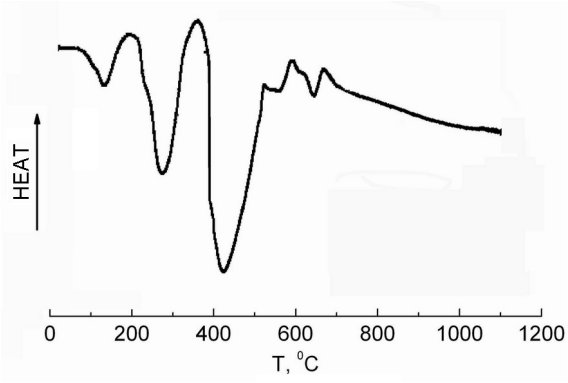

Fig. 1. DTA curve of the Y_2O_3 precursor obtained by deposition of yttrium salt by ammonium hydrocarbonate.

dispersion of the deposition products. The process of obtaining and characterization of Y_2O_3 nanopowder are described in detail in [10]. The sediment formed after the ageing, vacuum filtration and washing was dried in air and analyzed by means of DTA for determination of the regimes of precursor thermal treatment. The thermal treatment consisted of several steps at 150°C, 300°C and 450°C corresponding to the thermal effects on the DTA curve (Fig. 1) connected with stepwise loss of bound water as well as the hydroxyl and carbonate groups.

The diffraction patterns of the initial precursor and the powders after their thermal treatment at 150 C, 300 C and 450 C are presented in Fig. 2. In all the cases the duration of isothermal treatment was 10 h.

The system of reflections on the diffraction pattern of the powder subjected to thermal treatment at 450°C corresponds to the cubic structure of α-Y_2O_3 with an unit cell of 10.6140(4) Å (Fig. 2d). The size of the region of coherent scattering (RCS) calculated from the widening of the peaks of the X-ray pattern of Y_2O_3 powder is 17 nm (Fig. 3). The size of RCS and the morphology of the obtained Y_2O_3 powder are a good agreement with the data of [10].

The obtained Y_2O_3 nanopowder was used to produce compacts with a diameter of 20 mm by means of uniaxial pressing under a pressure of 200 MPa. Their density ranged between 50 and 60 % of the theoretical one of Y_2O_3. The compacts were sintered for 20 h at T = 1800–1850°C. Vacuum in an inductive heating furnace was $5 \cdot 10^{-3}$ Pa. The rate of heating and cooling of the samples was not higher than 50–100 deg./h. The samples of the Y_2O_3 and Y_2O_3:Nd (3 mass. % of Nd) ceramics prepared according to the described procedure

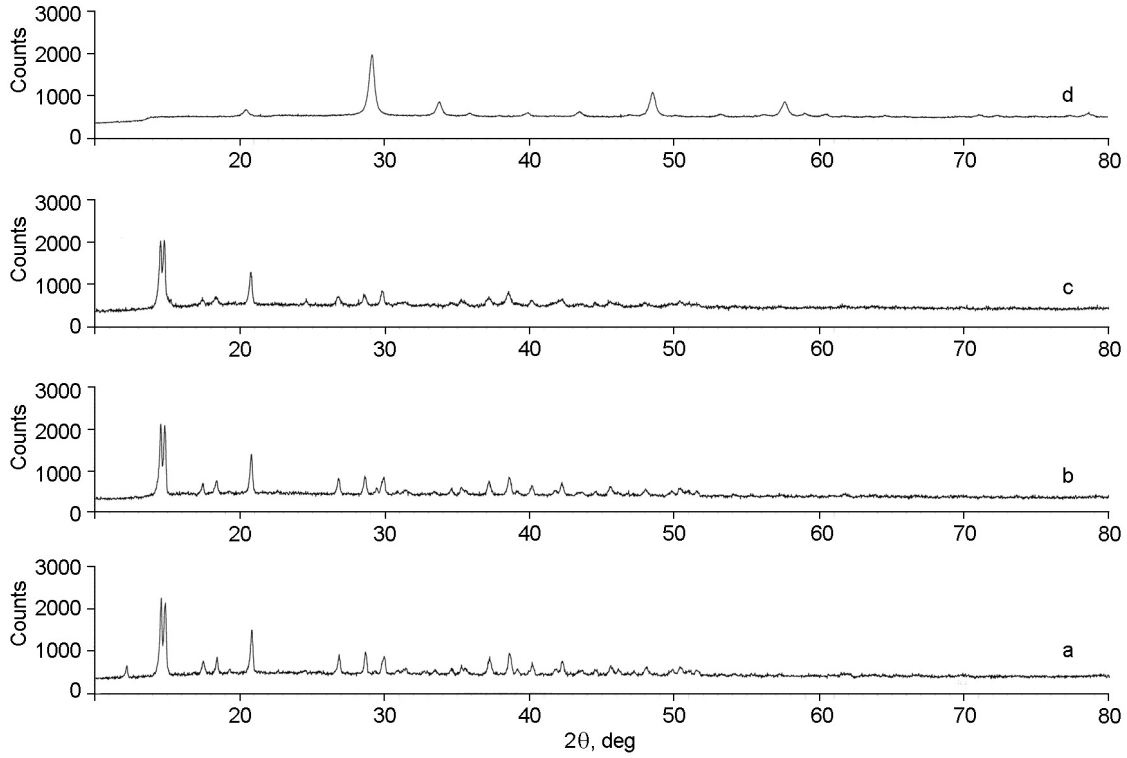

Fig. 2. X-ray diffraction patterns of the initial precursor Y_2O_3 (a) and of the thermally treated precursor: T = 150°C (b), T = 300°C (c), T = 450°C (d).

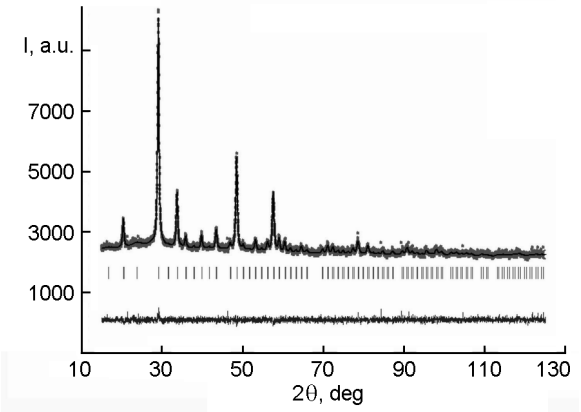

Fig. 3. Results of Rietveld refinement for X-ray diffraction pattern of the precursor Y_2O_3 after thermal treatment at 450°C. Solid line denotes the experimental curve, points correspond to the calculated data.

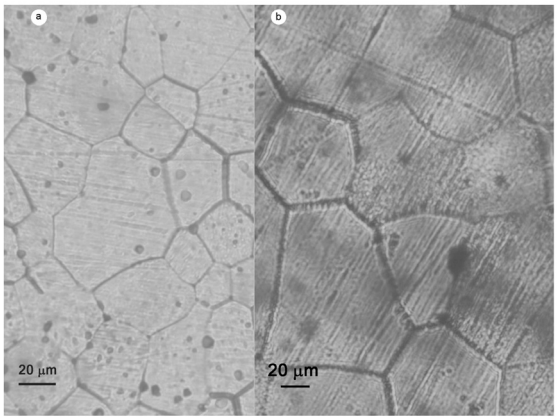

Fig. 4. Photograph of the surface of Y_2O_3 (a) and Y_2O_3:Nd (b) ceramics after etching.

had a density of 99.9 % of the theoretical one.

3. Results and discussion

3.1. Granulometric and phase compositions, crystal structure of Y_2O_3 ceramics

The obtained ceramics was found to consist of 20–80 μm crystallites. The average crystallite size in Y_2O_3:Nd samples is approximately by 1.5 times larger in comparison with that in the nominally pure Y_2O_3 ceramics. All the obtained ceramic samples are characterized by the presence of porosity (Fig. 4). The pores are randomly distributed at the boundaries of the crystallites or in their bulk. The concentration of residual pores in all the samples was ~1–2 vol. %.

According to the data of XPA, the ceramics is composed of the grains of the cubic α-Y_2O_3 modification. The unit cell parameter of the nominally pure sample of Y_2O_3 ceramics is in good agreement with the literature data [11].

Table 1. Unit cell parameters and phase composition of Y_2O_3 ceramics

	Unit cell parameters		Content of γ-Y_2O_3 phase, mass. %	Microstresses, %
	α-Y_2O_3	γ-Y_2O_3		
Y_2O_3	a = 10.60401(9) Å V = 1192.370(18) Å^3	a = 13.552(3) Å b = 3.5868(7) Å c = 8.5509(2) Å β = 99.931(18)° V = 400.25(17) Å^3	4.4	1.09
Y_2O_3:Nd	a = 10.61889(9) Å V = 1197.395(17) Å^3	a = 13.575(13) Å b = 3.5085(3) Å c = 8.5664(11) Å β = 99.992(8)° V = 401.84(7) Å^3	3.9	0.88

As found in our investigations, the pure ceramic samples and the ones doped with Nd contained the impurity of the monoclinic phase γ-Y_2O_3. Its concentration was approximately the same in all the samples — ~4 mass. %. The neodymium doping (R_Y = 0.97 Å, R_{Nd} = 0.98 Å) results in the substitution of yttrium and the formation of substitution solid solution. Thereat, the lattice parameter and the unit cell volume of the cubic and monoclinic phases increase (Table 1). Moreover, according to the data of X-ray structure analysis, all the samples have a high (~1 %) concentration of unit cells deformed due to microstresses (Table 1).

As it is known, the lattice parameter of metal nanoparticles is lesser than the one of the bulk material. The change of the unit cell parameter $\Delta a/a$ may run into 2 % depending on the metal and the nanoparticle size. For compounds the experimental data on the dependence of the lattice parameter on the nanoparticle size are ambiguous. The unit cell parameters have been observed both to decrease and to rise [12]. The interatomic distances may decrease due to violation of the stoichiometry (when the content of one of the components becomes lower), or adsorption of the impurities with ionic radii smaller than those of the matrix elements of the nanoparticle (for nitride nanoparticles) [13, 14]. Moreover, the lattice parameter may increase due to the presence of impurities in the nanoparticle, as it takes place for CeO_2 and MgO nanoparticles [15, 16].

In our case, for 17 nm Y_2O_3 nanoparticle the rise of the unit cell parameter is $\Delta a/a$ ~ 0.1 %. It is most probable that at "wet" synthesis of the nanoparticles the impurities are incorporated into the crystal lattice of Y_2O_3. Due to uniform distribution of the impurities in the nanoparticle bulk the unit cell parameter of the nanoparticle is larger, but not smaller, in comparison with that of bulk Y_2O_3 sample. At subsequent sintering of the compacts the impurities diffuse and reside at the grain boundaries. This is confirmed by different etching rate of the grain boundaries of the obtained ceramics (Fig. 4).

3.2. Mechanical properties of Y_2O_3 ceramics

The mechanical properties of the ceramics (its microhardness H_v and fracture toughness K_{1c}) were investigated by the method of indentation using Vickers diamond pyramid (PMT-3). The fracture toughness K_{1c} was calculated according to the formula [17]:

$$K_{1C} = 0.016(E/H_v)^{1/2} \frac{P}{C^{3/2}}, \quad (1)$$

where E is the Young's modulus, P — the applied load, C — the crack length. The values of microhardness and fracture toughness were determined at a load of 50 g.

The above-said characteristics are sensitive to the microstructure of the ceramics (its grain size, grain boundary perfection, size and concentration of pores, point defects). The existing data on the mechanical properties of the ceramics Y_2O_3 are contradictory. According to [11], the values of microhardness H_v and fracture toughness K_{1c} are practically constant for the ceramic materials with a grain size ranging between 0.2 and 214 μm. Moreover, these values are constant at loads up to 10 N. On the con-

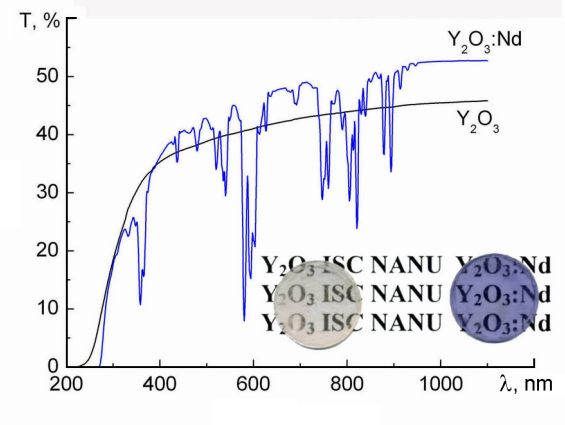

Fig. 5. Transmission spectra of Y_2O_3 and Y_2O_3:Nd ceramics. The insert contains the photograps of the samples.

trary, in [18] the authors report an increase of approximately 10 % for the microhardness and of 2.5 times for the fracture toughness observed in the Y_2O_3 ceramics with 1–2 μm grains in comparison with the ceramics with a grain size of 5–10 μm.

The value of microhardness H_v obtained in the present work is somewhat higher than the one of the HIP ceramics 8 GPa [19] and lower in comparison with the microhardness of the MIP ceramics 11.8 GPa [7] with the crystallites with a size of several ten micrometers. At the same time, the obtained fracture toughness is lower than that of the HIP ceramics — 3.5 MPa·m$^{0.5}$ and MIP — 1.4 MPa·m$^{0.5}$ (Table 2).

The ratio K_{1c}/H_v may be used as the parameter governing the "brittle-to-ductile" transition [11]. For the pure and doped samples of the ceramics Y_2O_3 the said ratio is practically the same. Thus, the doping with neodymium increases the microhardness H_v, the value of brittleness remaining practically unchanged.

3.3. Transmission of Y_2O_3 ceramics, Nd^{3+} luminescence and decay

The transmission spectra were measured by means of a CARY 5000 spectrophotometer. The luminescence spectra were studied using a monochromator MDR 23 (LOMO) pumped by a laser diode emitting at 802 nm wavelength. In the process of these measurements the spectral width of the monochromator slot was <1 nm. Nd^{3+} luminescence decay was studied by using LS 2137 laser coupled with parametric generator LT-2214 OPO (duration of pulse 15 ns), photoreceiver (InGaAs PIN diode) and Tektronics TDS 3052B digital oscillograph.

Table 2. Mechanical characteristics of Y_2O_3 ceramics

	Microhardness H_v, GPa	Fracture toughness K_{1c}, MPa·m$^{0.5}$	K_{1c}/H_v, $\times 10^{-3}$·m$^{0.5}$
Y_2O_3	8.92	0.83	0.093
Y_2O_3:Nd	9.49	0.87	0.092

The transmission spectra of Y_2O_3 and Y_2O_3:Nd ceramics with a thickness of 1 mm are presented in Fig. 5. As seen from Fig. 5, the transparency of the ceramic samples prepared under the described conditions was not lower than 55 %. The transmission spectrum of the sample Y_2O_3:Nd obtained in nonpolarized light contains a number of absorption lines caused by the transitions from the ground state $^4I_{9/2}$ of Nd^{3+} ions. The analysis of the lines in the absorption and luminescence spectra (Fig. 6) of the ceramic and single crystal [20] samples of Y_2O_3:Nd points to the difference in the intensity ratios for the Stark components of the corresponding f–f transitions. Such a behavior may be caused by nonequivalent local surrounding of neodymium in the crystal lattice of the single crystal and the ceramics and, consequently, by the change in the forces of the oscillators of the transitions f–f for Nd^{3+} ion [21]. The presence of optical centers with a lower local symmetry of Nd^{3+} ion was also reported for the ceramics Y_2O_3:Nd obtained by MIP [7].

The experimental curves of Nd^{3+} luminescence decay are to a high degree approximated by the two-exponential dependence:

$$I(t) = I_0 + I_1 e^{-t/t_1} + I_2 e^{-t/t_2}, \qquad (2)$$

where I_0 is the constant (background) component of the signal, I_1 and I_2, the maximum values of the signals with the decay constants t_1 and t_2, respectively. The data on the luminescence kinetics for the maxima at 0.94 μm, 1.07 μ and 1.35 μ are contained in Table 3. It should be noted that the obtained luminescence decay times for Y_2O_3:Nd ceramics are by an order lower in comparison with that for the single crystal: t_{cryst} = 300 μs [19]. This testifies to a considerable role of nonradiative transitions in the upper laser level emptying, since $t_{cryst} > t_1, t_2$.

Table 3. Nd^{3+} luminescence ($^4F_{3/2} \rightarrow {}^4I_{9/2,\ 11/2,\ 13/2}$) decay times in Y_2O_3 ceramics

Decay time	Position of luminescence maximum λ_{max}, μm		
	0.94 ($^4F_{3/2} \rightarrow {}^4I_{9/2}$)	1.07 ($^4F_{3/2} \rightarrow {}^4I_{11/2}$)	1.35 ($^4F_{3/2} \rightarrow {}^4I_{13/2}$)
t_1, μs	12.4	51.6	52.4
t_2, μs	46.1	15.3	18.4

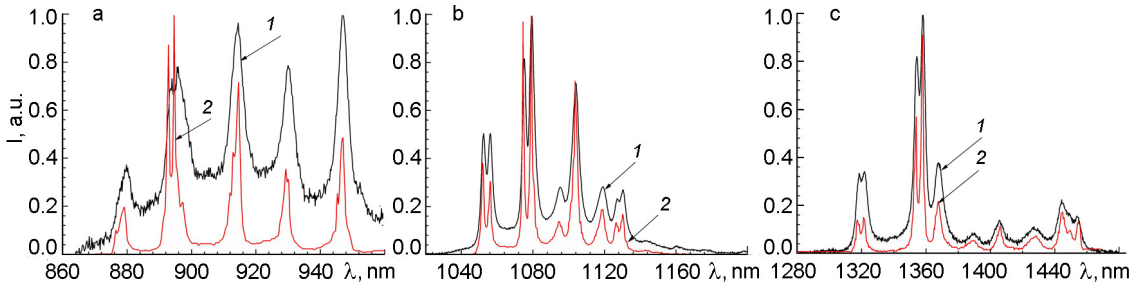

Fig. 6. Normalized luminescence spectra of Y_2O_3:Nd ceramics (*1*) and single crystal (*2*) [19]. Nd^{3+} *f–f* transitions: (a) — $^4F_{3/2} \rightarrow {}^4I_{9/2}$, (b) — $^4F_{3/2} \rightarrow {}^4I_{11/2}$, (c) — $^4F_{3/2} \rightarrow {}^4I_{13/2}$.

4. Conclusions

Thus, the assumption of the existence of two nonequivalent centers Nd^{3+} in Y_2O_3 ceramics is confirmed by the X-ray structure analysis data on the change in the lattice constant and the volume of the unit cell of the cubic and monoclinic phases at the doping with neodymium (Table 1), as well as by the spectral-kinetic characteristics.

The authors are grateful to Dr.E.F.Dolzhenkova, Dr.A.V.Lopin, and Dr.V.F.Tkachenko for fruitful discussions during preparation of the manuscript. The work is fulfilled in the frames of SFFR-BRFFR Joint Project F41.2/0.19.

References

1. Advances in Ceramics — Synthesis and Characterization, Processing and Specific Applications, ed. by C.Sikalidis, InTech, Croatia (2011).
2. A.A.Kaminskii, M.Sh.Akchurin, R.V.Gainutdinov et al., *Kristallografiya*, **50**, 935 (2005).
3. A.A.Kaminskii, *Laser & Photonics Rev.*, **1**, 93 (2007).
4. Japan. Patent 10-101411 (1998).
5. X.Hu, Q.Yang, C.Dou et al., *Opti.l Mat.*, **30**, 1583 (2008).
6. Yu.L.Kopylov, V.B.Kravchenko, S.N.Bagayev et al., *Optical Materials*, **31**, 707 (2009).
7. S.Bagaev, V.Osipov, M.Ivanov et al., *Photonics*, **5**, 24 (2007).
8. T.Ikegami, Ji-Guang Li, T.Mori, *J.Am.Ceram. Soc.*, **85**, 1725 (2002).
9. J.Rodriguez-Carvajal, T.Roisnel FullProf.98 and WinPLOTR: New Windows 95/NT Applications for Diffraction. *Commission for Powder Diffraction, International Union of Crystallography, Newsletter* No.20 (May-August) Summer 1998."
10. V.N.Baumer, T.G.Deineka, T.A.Korshikova et al., *Crystallography Rep.*, **53**, 1191 (2008).
11. G.Fantozzi, G.Orange, K.Liang et al., *J.Am. Ceram.Soc.*, **72**, 1562 (1989).
12. A.I.Gusev, Nanocrystalline Materials: Methods of Obtaining and Properties, Urals Dep. of RAS, Yekaterinburg (1998) [in Russian].
13. V.F.Petrunin, Yu.G.Andreev, V.N.Troitskiy et al., *Poverkhost*, **11**, 143 (1982).
14. V.F.Petrunin, Yu.G.Andreev, T.N.Miller et al., *Poroshkovaya Metallurgiya*, **9**, 90 (1987).
15. M.Ya.Gamarnik, *Solid State Physics*, **30**, 1399 (1988).
16. A.Cimino, P.Porba, M.Valigi, *J.Am.Chem. Soc.*, **409**, 152 (1966).
17. G.R.Anstis, P.Chantikul, B.R.Lawn, D.B.Marshall, *J.Am.Ceram.Soc.*, **64**, 533 (1981).
18. A.S.Kaigorodov, V.V.Ivanov, V.R.Khrustov, A.I.Medvedev, *Perspektivnye Materialy*, **2**, 36 (2007).
19. M.Desmaison, J.Montinin, F.Valin, M.Boncoeur, *J.Am.Ceram.Soc.*, **78**, 716 (1995).
20. B.M.Walsh, J.M.McMahon, W.C.Edwards et al., *J.Opt.Soc.Am.B*, **19**, 2893 (2002).
21. I.A.Belova, F.A.Bolshchikov, Yu.K.Voron'ko et al., *Solid State Phys.*, **50**, 1552 (2008).

Вплив умов отримання на структуру та властивості кераміки оксиду ітрію

В.М.Баумер, М.Б.Космина, Б.П.Назаренко, В.М.Пузіков, О.М.Шеховцов, Л.С.Гордієнко, А.С.Ясюкевич, М.В.Кулешов, О.Є.Гулевіч, М.П.Демеш

Методом "мокрої" хімії отримано нанопорошок Y_2O_3, який охарактеризовано методами рентгенівської дифракції та диференційно-термічним аналізом. Спіканням у вакуумі отримано прозору кераміку Y_2O_3 і Y_2O_3:Nd. Вивчено кристалічну структуру, гранулометричний і фазовий склади, спектрально-кінетичні та механічні властивості отриманої кераміки.